OPEN ACCESS
IOP Publishing
Semiconductor Science and Technology
Semicond. Sci. Technol. **34** (2019) 083001 (14pp)
https://doi.org/10.1088/1361-6641/ab2838

Topical Review

Multi-wavelength distributed feedback quantum cascade lasers for broadband trace gas spectroscopy

Mehran Shahmohammadi[1,4], Filippos Kapsalidis[1], Martin J Süess[1], Emilio Gini[3], Mattias Beck[1], Morten Hundt[2], Béla Tuzson[2], Lukas Emmenegger[2] and Jérôme Faist[1]

[1] Institute for Quantum Electronics, ETH-Zürich, CH-8093 Zürich, Switzerland
[2] Laboratory for Air Pollution and Environmental Technology, Empa, CH-8600 Dübendorf, Switzerland
[3] FIRST-lab Center for Micro- and Nanoscience, ETH-Zürich, CH-8093 Zürich, Switzerland

E-mail: smehran@phys.ethz.ch and jerome.faist@phys.ethz.ch

Received 9 July 2018, revised 28 March 2019
Accepted for publication 10 June 2019
Published 5 July 2019

Abstract

We review the progress of multi-wavelength distributed feedback (DFB) quantum cascade lasers (QCLs) as sources for broadband mid-infrared (mid-IR) spectroscopy. While it is possible to tune the emission wavelength of DFB QCLs in a frequency range of about 5 cm^{-1} by varying the operating temperature and driving current, continuous, deterministic and mode-hop free tuning remains challenging. To use these laser sources for broadband spectroscopy applications and to exploit their narrow linewidth, the equalization of the power across the multicolor spectrum is another requirement. Various approaches are reviewed: conventional DFB QCL arrays, surface emitting DFB QCL arrays, on-chip beam combined DFB arrays, multi-channel Vernier-based switching DFBs, and dual-wavelength DFBs. The results are presented to highlight the applicability of these sources for broadband and high-resolution trace gas spectroscopy. The results for multi-species trace-gas spectroscopy using dual-wavelength QCLs are presented in more detail, where the best precision as determined from Allan-Werle plots was obtained for measurement of NH_3 with 0.02 parts per billion (ppb) at 100 s integration time, and typical values for the other trace gases of the order of 0.1 ppb. These results indicate that spectrometers using dual-wavelength QCLs can serve as an all-in-one solution for high precision gas spectroscopy.

Keywords: multiwavelength QCLs, Multi-species trace gas sensing, quantum cascade laser arrays, distributed-feedback (DFB) QCL, Mid-infrared, semiconductor lasers

(Some figures may appear in colour only in the online journal)

1. Introduction

Quantum cascade lasers are unipolar intersubband devices, emitting in the mid-IR and THz parts of the electromagnetic spectrum [1, 2]. In contrast to interband lasers, in which the gain is always accompanied by absorption at higher frequencies, the intersubband active regions can be designed

[4] Author to whom any correspondence should be addressed.

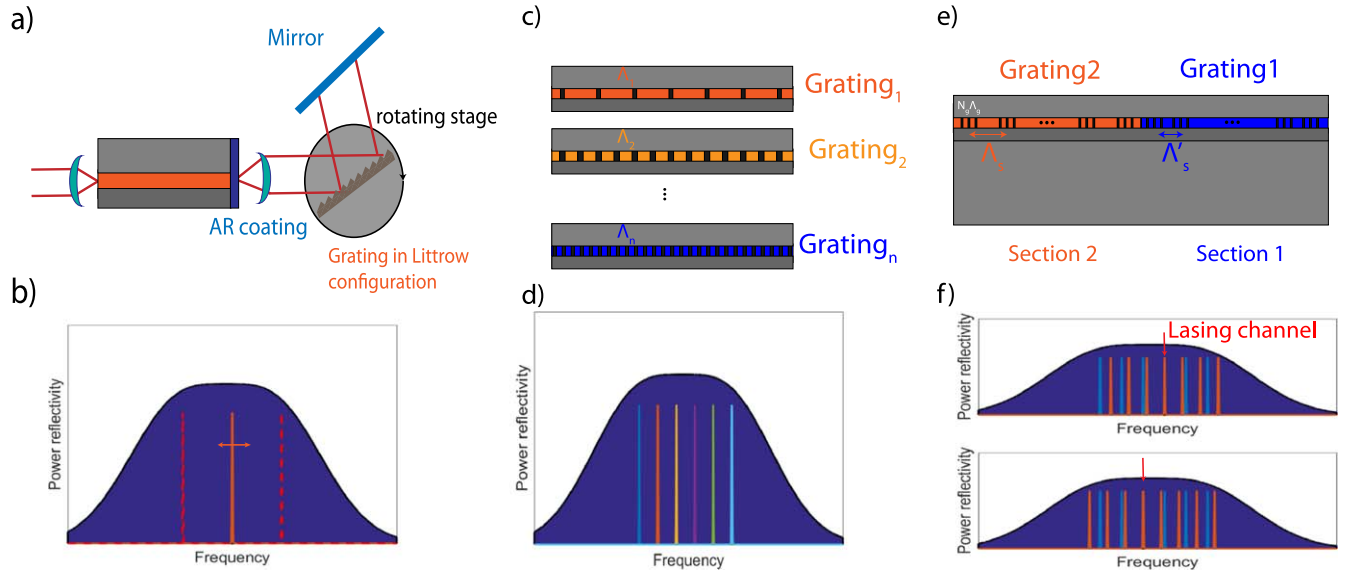

Figure 1. Schematic showing the operation principle of the three main broadband and single mode QCL sources: (a) External cavity QCL in Littrow front extraction configuration, where the 1st order diffracted beam is reflected back into the QCL. (b) The gain curve of QCL (shown in blue), and the lasing frequency marked by a narrow solid line, which can be tuned over the range of the gain spectrum frequency. (c)–(d) Schematic of a DFB QCL array, where the grating periodicity on each DFB QCL is different and therefore each DFB QCL element lases at different frequency as shown in different color in (d). Despite the narrow width of tuning of each element, the lasing spectrum of array can cover wide range of spectrum of the gain. (e) Schematic of a Vernier tuning DFB QCL, consisting two sections, each with an integrated sampled grating with corresponding grating periodicities Λ_g that is sampled at periodicities Λ_s (Λ'_s) in the front (back) section of the device. The slight differences in the periodicity of sampling of gratings leads to slight differences in the reflectivity of each section, shown by blue and red in part (f). (f) Upper panel shows the reflectivity of the two sections in absence of heating, where the arrow marks the aligned reflection channel and therefore the favorable lasing channel. Lower panel shows the switching mechanism, where the reflectivity of one of the mirrors (orange one) is red-shifted and therefore the aligned reflection channel and the favorable lasing channel of laser is switched.

such that they exhibit a large window of transparency. As a result, they offer excellent tailoring of their spectral gain by band structure engineering of the active region and stacking cascades of different gain profiles [3, 4]. In addition, they provide the possibility of precise mode control via distributed feedback (DFB) and distributed Bragg reflector (DBR) gratings [5–7]. Thanks to the small Henry's linewidth enhancement factor of DFB QCLs, these lasers have been shown to have a low white frequency noise, and therefore narrow intrinsic linewidth described by the Schawlow-Townes limit [8–10]. Their performance in the mid-IR range, in which one can access the fundamental ro-vibrational transitions of many pollutant and greenhouse gas molecules, makes them the preferred choice for laser-based trace gas sensing applications [11–14].

As compared with the beam combination of multiple single frequency devices [15–17], multi-wavelength QCLs can bring a substantial simplification to the optical designs and hence to realize more robust, compact, and cost-effective multi-component gas spectrometers [14, 18]. In order to realize broadband spectral coverage in mid-IR, QC active regions with a broadband gain and equalized intensity are required [3, 4, 19]. Another prerequisite is a mode control scheme that allows wavelength selection and tunability over this broadband gain spectrum. The approaches for realization of broadband and single mode QCLs can be categorized in three main types: (i) external-cavity QCLs, where the emission mode is controlled by an optical filter consisting usually of a grating in the Littrow configuration [4, 20, 21] (figures 1(a)–(b)), (ii) multi-wavelength DFB QCL arrays, where multiple electrically switched single/multimode DFB QCLs are arranged such that they cover multiple target wavelengths with either continuous or discrete spectral coverage [5, 22, 23] (see figures 1(c)–(d)), and (iii) multi-channel DFB QCLs, where thermal tuning combined with Vernier effect is used to switch the lasing channel and which optimal designs can cover the gain spectrum in continuous and discrete tuning mode (figures 1(e)–(f)). Dual-wavelength DFBs discussed in this review, can be considered as special case of (ii) or (iii). Not all types of single mode QCL emitters, such as single mode QCLs based on asymmetric Mach–Zehnder interferometer structures [24], are covered in this review since there are no demonstrations of broadband tuning of those sources. QCL frequency combs are the other broadband QCL sources that have been demonstrated to be powerful sources for spectroscopy with very narrow intrinsic linewidth and broadband emissions [25–27]. Gas spectroscopy applications using frequency comb QCLs are evolving very fast, but require relatively sophisticated data acquisition, laser driving and data corrections and thus fall outside the scope of this review [26, 28, 29].

External cavity QCLs have the advantage of broad tunability and a single output optical beam that eases the interface with the rest of the optical setup (see figures 1(a)–(b) for detail). However, the mechanically controlled frequency tuning rate of these laser sources, which is in the range of 0.1 to 25 cm^{-1}/ms for state-of-the-art commercial devices [21], and $<1000\,cm^{-1}$/ms for the fastest ones based on acousto-optic

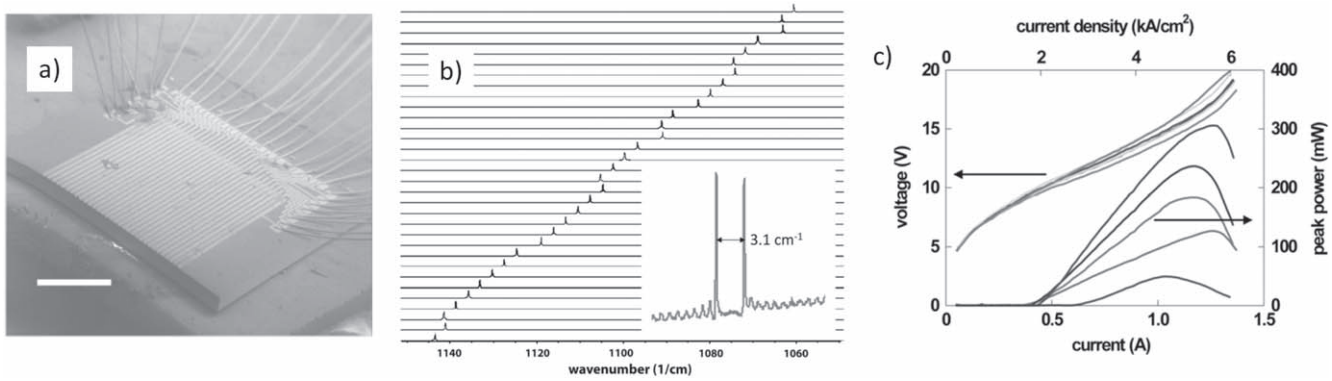

Figure 2. (a) SEM image of a fabricated DFB QCL array chip, consisting of 32 DFB QCLs. (b) Spectra of each element of the DFB QCL array, spaced in frequency by ~2.75 cm^{-1} over a span of ~85 cm^{-1}. Inset: the two modes on either side of the photonic bandgap, where the spacing is a measure of the coupling strength of DFB grating. When single mode operation is achieved, side mode suppression ratio (SMSR) was measured to be >20 dB. (c) Light-current-voltage (LIV) characteristic of the array elements: while the threshold currents of most of elements are similar, the slope efficiency and therefore the peak output power varies significantly. Adapted with permission from [33].

modulators [30], limits the spectroscopy of gas species with distant absorption features. More importantly, the mechanical tuning of external cavity QCLs causes low repeatability and accuracy of their wavelength (typically for commercial external cavities >0.1–0.5 cm^{-1}) which limit their application for high-sensitivity gas spectroscopy measurements.

In this review, we focus on approaches using DFB QCLs for realization of sources for mid-IR spectroscopy. Due to the limited tuning range of DFB QCLs (typically <5 cm^{-1}), multiplexing of DFB QCLs has been extensively explored over the past years in order to realize broadband mid-IR sources. Indeed, the limitation to very few compounds within the spectral coverage of a single DFB laser can be overcome by rapid time-multiplexing of several single-wavelength QCLs. This approach has the advantage of high selectivity and sensitivity in each DFB QCL tuning window as well as being compatible with fast electrical switching. In the following, we review and compare different design architectures with focus on the application in multi-component trace-gas sensing.

2. DFB QCL arrays and MOPAs

The first realization of DFB QCLs with different emission wavelengths on a single active region was demonstrated in 2006 [31]. Employing first-order DFB gratings with different periods to an active region with a bound-to-continuum design allowed single mode continuous wave emission at several wavelengths ranging from 7.7 to 8.3 μm at a temperature of +30 °C. In 2007, the demonstration of a multi-wavelength DFB QCL array was reported with an array of 32 DFB QCLs operating between 8.7 and 9.4 μm on a chip [32] (see figure 2). The broadband coverage (~85 cm^{-1}) was achieved by a combination of electrical switching and thermal tuning. In order to have deterministic control over the lasing frequency range of individual QCLs, a strongly over-coupled grating was used ($\kappa L \sim 11$, where κ and L are the grating's coupling strength and the device length, respectively). In this way, the effect of the end facet mirrors on the mode selection (see for detail [33, 34]) was effectively suppressed and all the lasers of the single array were lasing in single-mode and all on the high-frequency side of the photonic gap formed by the DFB gratings. The slope efficiency of the reported array, however, had variation of one order of magnitude (from 20 mW/A to 200 mW/A) over its optical bandwidth. This variation of the slope efficiency was attributed to the random position of the cleaved laser facets with respect to the gratings, as described later in [35], as well as the non-uniform injection over the laser ridge due to the deeply etched DFB gratings. A later realization with an extended broadband operation up to 200 cm^{-1} and improved equalization of the output power (the slope efficiency varying between 250 and 2500 mW/A) [35] still suffered from this problem. These DFB arrays were employed for spectroscopy measurements of liquid phase of methanol, acetone, or isopropanol in [33]. The broad absorption lines of the mentioned gases were measured either by pure switching of DFBs or by a combination of electrical switching and temperature tuning.

The same approach was employed by other groups [19], where 6 stacks of discrete wavelength quantum cascade stages, emitting at 5.9–10.9 μm, were stacked to realize a ~760 cm^{-1} broadband active region (see figure 3(a)). A uniform threshold current density across the lasing spectrum was demonstrated on a DFB array consisting of 24 QCLs. The peak output power (1% duty cycle pulse driving condition) was varying significantly on the edge of the gain bandwidth. The single mode emission under pulse condition was obtained over a significant portion of spectral range. The peak power variation was attributed to the unbalanced gain over the design spectrum, and, similar to the previous demonstrations, to the strong variation of κL over the design spectrum. Whereas, the inhomogeneity of the gain across the target optical bandwidth can be corrected by improvement of the active region design or redistribution of the stacked active region, for a given length of a DFB array, compensation of the spectral variation of the coupling strength requires relatively sophisticated anti-reflective coatings.

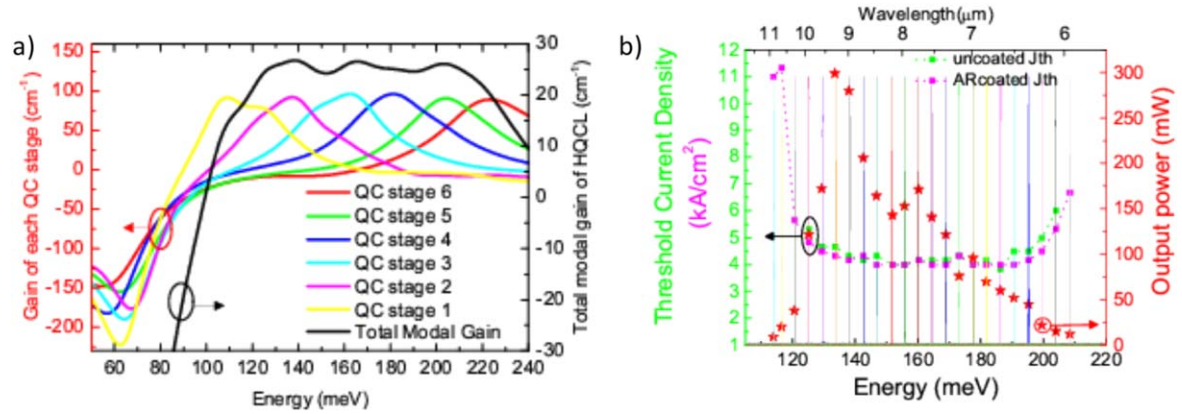

Figure 3. (a) Simulation of the gain profile of the individual QC stacks and the total modal gain (black), at a current density of ~4 kA cm^{-2}. (b) Threshold current density for uncoated (green), and anti-reflective coated (pink), as well as the output peak power as a function of emission energy (Pulses of 200 ns width and a duty cycle of 1%). Adapted from [19]. CC BY 4.0.

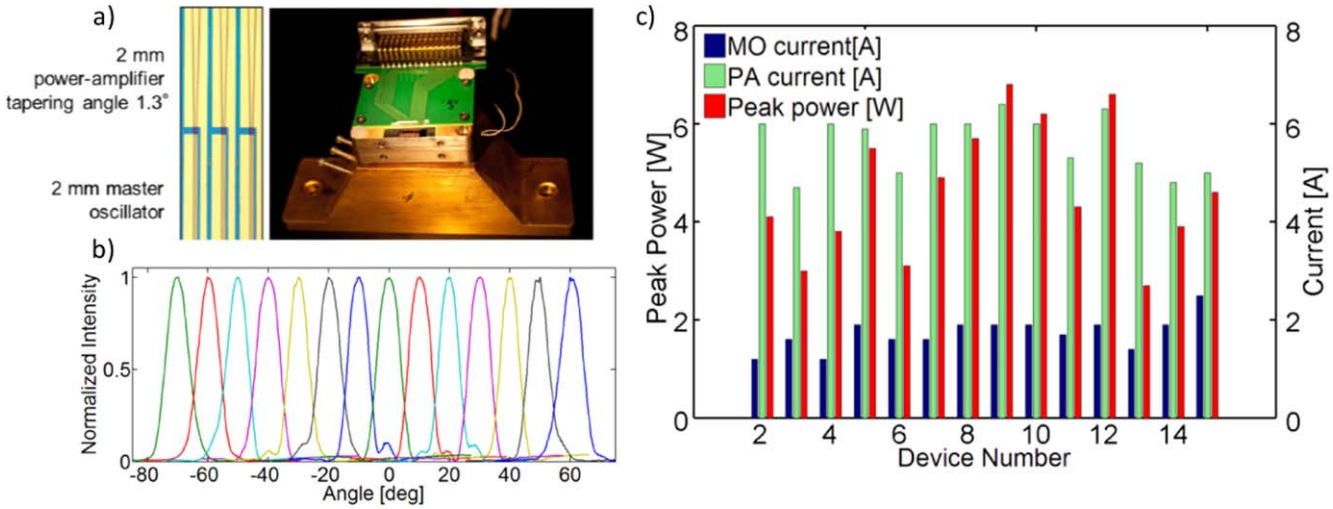

Figure 4. (a) The elements of a MOPA array with 2-mm-long DFB section and an equally long tapered power-amplifier with a taper angle of 1.3° as well as the packaged array, allowing individual electronic addressing of both device sections for all of the array elements. (b) Angular in-plane distribution of the far-field intensity for all devices. The devices were operated at maximum single-mode power. The plots have been offset horizontally for clarity. (c) Performance of MOPA array at optimum driving condition: The values for master-oscillator (blue bars) and power-amplifier peak currents (green bars) together with the corresponding peak power values (red bars). Adapted from [6]. CC BY 4.0.

In order to overcome the peak power variation in DFB arrays, master oscillator power amplifiers (MOPAs) have been considered, which consist of a master oscillator section to generate a single mode TM_{00} mode and a power amplification section [36]. The two sections are electrically isolated in order to be biased with different current densities. This feature allows equalizing the output power of the array over its operation bandwidth. High peak output powers varying between 2.7 W to 10 W was reported for the single mode operation condition with optimum value of the bias current in the master oscillator and power amplifier section (see figure 4(c)) [6]. High SMSR of >20 dB was reported at the wavelengths ranging between 9.2 and 9.8 μm (~70 cm^{-1}), when single mode emission was achieved [36]. The proper design of the power amplifier section allows individual devices to exhibit single-lobed far-field characteristics with an average FWHM angle of the narrow in-plane intensity distribution of 7.7° (see figure 4(b)). The reported values for the single mode output power of the MOPA array in figure 4(c) were characterized by gradually increasing both the master oscillator and power amplifier currents up to a point, where single-mode operation was compromised due to lasing at additional modes. The multimode operation (as reviewed in [36]) can be attributed to either the multi-mode seeding in the master oscillator section (limited single mode emission dynamic range of master oscillator section) or the self-lasing in the power amplifier section at high injection currents. The evenness of the frequency of the arrays was limited to the lack of the control on the lasing of each element on the either side of the DFB photonic band gap, and was varying between 3.1 and 6.1 cm^{-1} [6, 37]. The multimode operation caused by the facet effects in MOPA arrays was shown to be even stronger than DFB arrays with anti-reflective coatings on the front facets. This is due to the fact that

any residual facet reflection can be amplified in the power amplifier section. Therefore, the authors proposed improvement of the anti-reflective coating, application of anti-reflective coating to both back and front facets, or using over-coupled DFB gratings similar to [33]. Introducing a defect into the photonic bandgap of the DFB section, called quarter-wave-shifted (QWS) DFB, can lead to the lasing mode in the middle of the photonic gap. The QWS design can strongly localize the optical field in the middle of the DFB section and therefore can reduce the effect of the facet. Although, the QWS DFB QCLs were successfully demonstrated as a solution for having deterministic lasing frequency in diode lasers [38, 39], good anti-reflective coatings seem to be a prerequisite in midIR QCLs. The later attempts by the same group showed no improvement on the mode selection control, while still a considerable portion (~25%) of the elements of the array were lasing on the either side of the photonic bandgap and not on the defect mode [37]. Moreover, the QWS design showed lower output peak power than MOPA arrays without QWSs, which varied between 0.8 and 3.9 W.

The MOPA arrays feature considerable improvement in the output power compared to conventional DFB arrays, but at the cost of less mode control. The two sections of MOPA arrays, or even three in case of the QWS DFB QCLs with an additional absorber section, add to the complexity of the driving electronics for these arrays compared to conventional DFB arrays. In order to simplify the electronic driving, another design called DBR/tapered oscillator array, was reported later by the same group [40]. The design is essentially the same as the MOPA array with the only difference that all devices are pumped at the same current. This design showed a lower single mode dynamics range since the facet of the tapered section makes a Fabry–Perot cavity which allows lasing on the side modes.

Most of the measurements reported so far from MOPA DFB arrays or tapered DFB arrays were performed with low duty cycle and short pulses (for instance in [36]): 10 kHz repetition rate and small duty cycle of 0.025% at a heat sink temperature of 18 °C). The short pulse operation condition however does not insure the performance of these arrays in terms of the output power, single mode emission dynamic range and particularly the mode-hop free tuning in continuous wave or intermittent continuous wave operation. The mode-hop free tuning is of crucial importance to perform high-resolution spectroscopy exploiting the narrow linewidth of DFB QCLs [41]. Therefore, the difficulty in insuring continuous single mode tuning of all array elements makes high resolution spectroscopy using MOPA arrays challenging but these sources have great potential for spectroscopy of liquids or heavy molecules with broad spectral features [33].

Even though, the beam quality was improved in MOPA arrays or the tapered DFB arrays for each single device [42], spectroscopy applications that demand long optical path cells require the combination the whole array emission in a single collimated beam. Using a single lens, as is done conventionally in front of the array, leads to large variation of the pointing angle of the output beam [34]. The wavelength beam combing using a single [43] or double grating scheme [44] can lead to much smaller pointing errors of 2 mrad or 0.2 mrad, respectively. The power losses due to the mismatch of the laser polarization and gratings was estimated to be less than 30% [34].

3. Surface emitting DFB arrays

Surface emitting ring cavity QCL arrays were reported in [22], where each element consists of a ring cavity with radial second-order Bragg gratings etched into the top cladding. In contrast to edge emitting DFB arrays, due to the absence of facets in the ring cavity QCLs, the performance of ring cavity QCL arrays is mainly determined by the incorporated gain material and is not affected by the underlying frequency selection mechanism. The results in [22] showed only little wavelength to wavelength power variations (from 20 to 60 mW) over a bandwidth of 180 cm^{-1}. The output power spectrum was shown to follow the gain profile of the active region (see figure 5(b)). The main challenges of ring cavity surface emitting arrays lie in the low output power and in the beam combination which has to account for the two dimensional design and the large footprint of these devices [34]. The narrow far-field and the 2D array geometry is, however, well suited to match with a microbolometer camera. The same group has also demonstrated a highly integrated mid-IR remote sensor consisting of quantum cascade lasers and detectors on the same chip with efficient mutual communication of the laser and detector and proof-of-principle gas measurements with a limit of detection below 400 ppm [45, 46].

Surface-emitting QCL arrays using DBRs together with a second order extractor have been also reported by our group [23]. The spectral coverage of 175 cm^{-1} and peak power of <2 mW was demonstrated as a proof of principle in 8–10 μm range. The far-field featured an acceptable value of 8.3° and 18.3° in the transverse and longitudinal direction, respectively. The main drawback of this approach was the limited output power (see figure 5(d)). The latter was mainly caused by the current leakages, the limited bandwidth and the low outcoupling efficiency of the second order gratings used to extract the emission of the array.

4. Vernier based switching DFB laser

Integrated sampled grating reflectors using the Vernier effect, have been used to extend the tuning range of semiconductor lasers diodes [47, 48]. This approach was successfully applied to QCLs with multiple sections [49–52]. In [50], the device was current-tuned between ten single modes spanning 63 cm^{-1}, from 8.32 to 8.78 μm. The peak optical output power exceeds 280 mW for nine of the modes. In this design as shown in figure 6(b), the switching of the lasing channel and tuning is performed by the current in the front or back section of the laser (labeled as SGR1, SGR2 in the figure 6(a)). For instance for the spectral tuning shown in part (b), the SGR1 is biased at fixed current and therefore temperature tuned continuously. SGR2 section is, however,

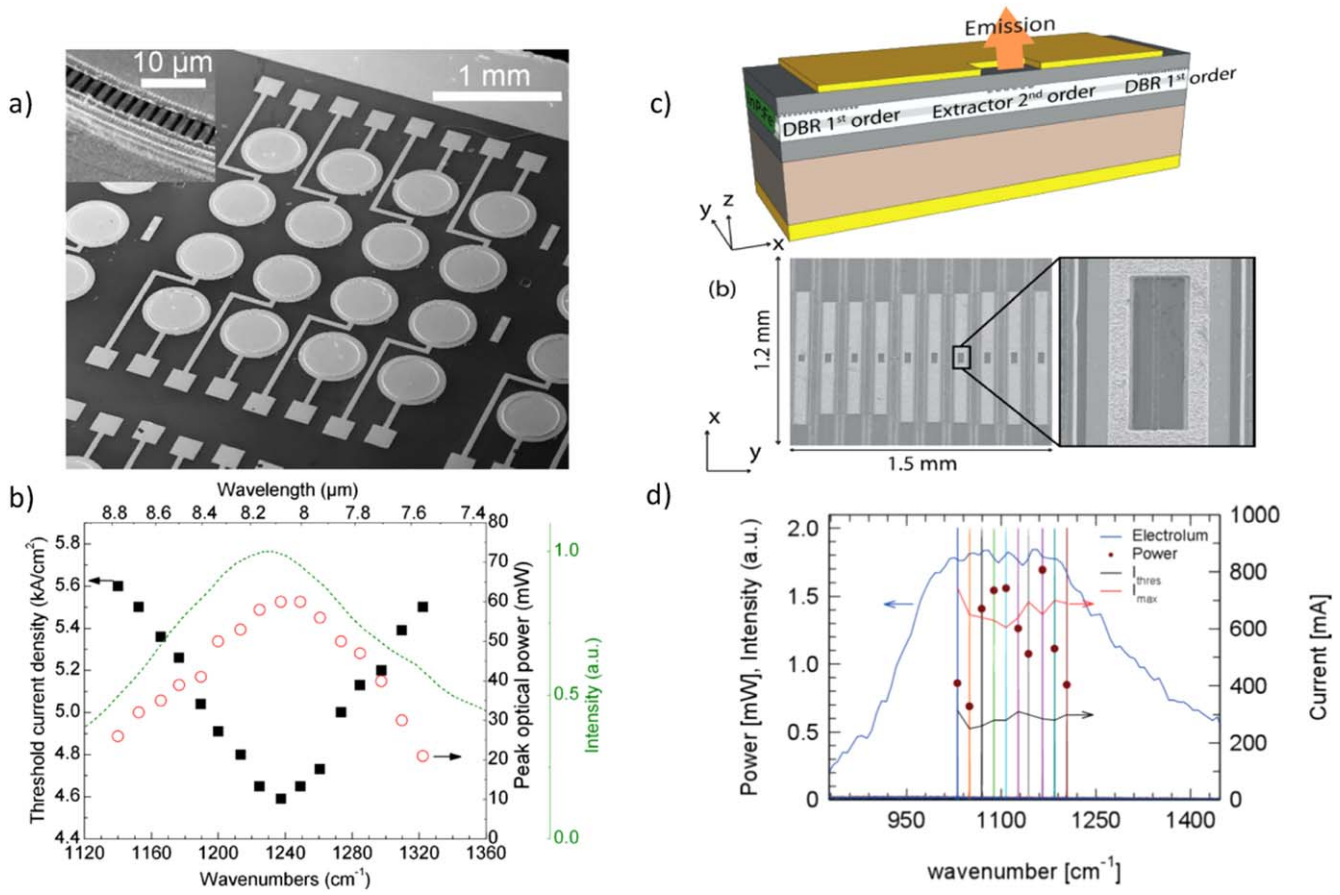

Figure 5. (a) SEM image of a surface emitting ring cavity QCL array, consisting of 16 elements. (b) Threshold current density (squares) and peak optical power (circles) as a function of the wavelength. The measured electroluminescence from a mesa (dashed line) indicates the gain spectrum of the incorporated QC material at 293 K. (c) Schematic drawing and SEM image of a surface-emitting QCL array using distributed Bragg reflectors together with a second order extractor. (d) Performance of a ten-lasers array measured in pulsed operation (1% duty-cycle with 30 ns pulses at T = 20 °C). The threshold and roll-over currents are reported for each element as well as the maximum peak power. On the same graph is shown the measured spontaneous emission of a similar device at room-temperature from the side to avoid any cavity or wave-guiding effects while driving the device at 13.5 V with a 6% duty cycle. (a)–(b) adapted from [22], and (c)–(d) from [23], with the permission of AIP Publishing.

switched on with short pulse at a delay t_{del}. Depending on the time delay, and therefore the relative frequency shift of the back/front section mirror's reflectivity with respect to its counterpart, the lasing channel is selected. Although one can realize switching and tuning of these lasers, the required sophisticated electronic driving limits this approach for spectroscopy applications.

Similar structures have been realized in [53], where the sampled grating DFB laser source is comprised of a series of short gratings periodically sampled on the two sections (figure 6(c)). Continuous wave operation at room temperature with frequency tuning up to 50 cm^{-1} at 4.8 μm was demonstrated for these lasers. The tuning range of each sampled grating DFB was demonstrated to be about one order of magnitude larger than the tuning range of the conventional DFBs. The mean SMSR of the sampled grating DFBs was shown to be ~24 dB, and the output power was exceeding 100 mW.

In the two presented Vernier extended tuning DFB QCL designs, the switching from one Vernier channel to the other is controlled via bias current in the laser sections. This indeed affects both the shift of the DBR stop bands and the output power. Since one important prerequisite for many gas spectroscopy applications is the sources with continuous tuning capability, the sophisticated electronic driving required for these designs limits their applications.

The later design in [54] provides more degrees of freedom in switching the lasing channel and tuning the lasing wavelength owing to the integrated heaters (see figure 6(e)). In fact, the existence of the integrated resistor heaters buried close to the active region allows to switch the different channels of the Vernier grating by applying the required temperature difference ΔT between the front and back section of the laser. The bias current of the laser section (both front and back section) can then thermally tune the selected channel by heater. This is shown for instance in figure 6(f), where the laser and integrated heater were used as two independent control knobs to tune the laser emission quasi-continuously over ~20 cm^{-1}. The design was successfully demonstrated at three different wavelength, i.e. 9.25 μm, 8.5 μm, and 4.4 μm, with continuous wave output power of few tens of mW.

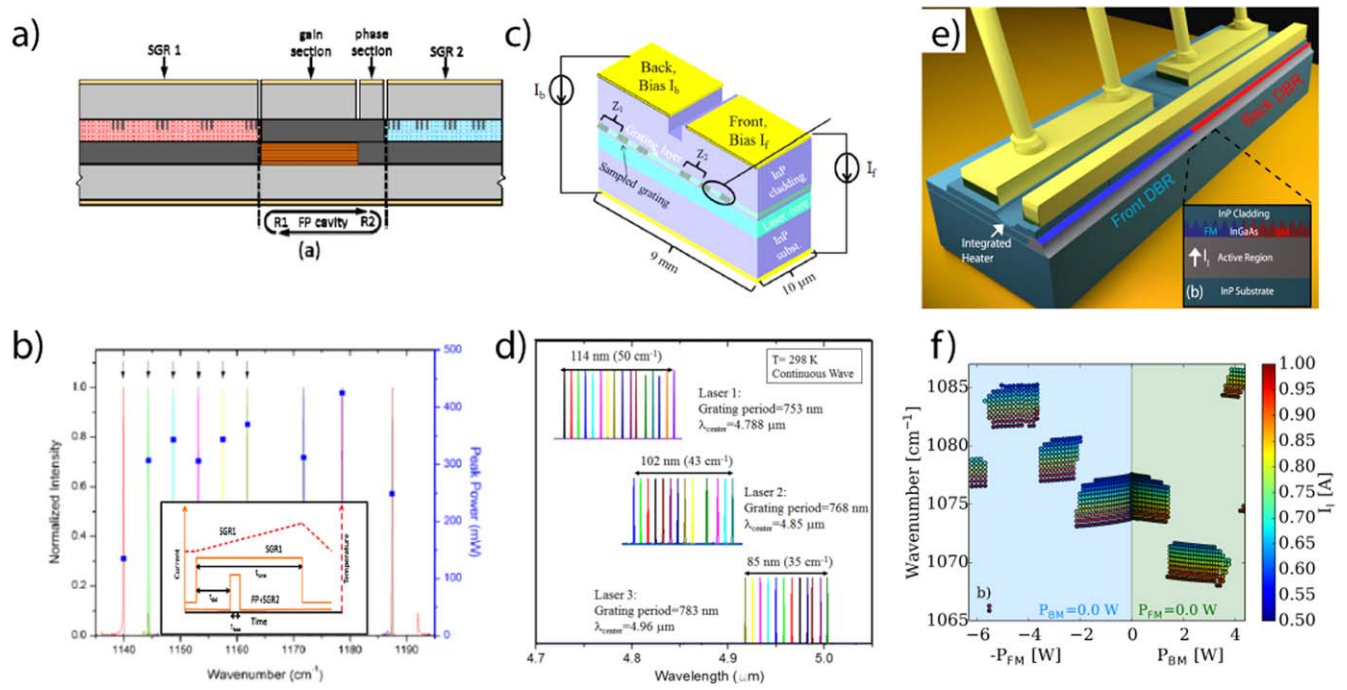

Figure 6. (a) Schematic of a typical sampled grating DBR laser, consisting of two sampled grating reflectors (SGR) with slightly different super-periods on each side of a Fabry–Perot (FP) cavity. The phase section controls the round-trip phase accumulation, which is critical for continuous tuning, but is not included here. Traditionally, the gain medium (orange) is restricted to the gain section and the facets are anti-reflective-coated, but here the SGRs also have gain and the facets are left uncoated. (b) Experimentally measured single modes, taken at different values of the applied currents and delay. Here, SGR1 is temperature tuned as discussed in the text. The ten single modes span a range of 63 cm^{-1}. Inset: Experimental approach to achieve discrete tuning. (a)–(b) adapted from [50], © 2012 Optical Society of America. (c) Schematic of a SGDFB device structure. (d) Room temperature, continuous wave, single-mode emission spectra for three lasers with different grating periods from the same wafer. A gap-free electrical tuning range of 120 cm^{-1} is demonstrated. (c)–(d) adapted from [53], with the permission of AIP Publishing. (e) Schematic drawing of the Vernier tuning DFB QCL. (f) mode maps for the device at T = 0 °C. On the horizontal axis, the electrical power pumped in the back or front (negative values) heaters is shown. (e)–(f) adapted from [54], with the permission of AIP Publishing.

Vernier based switching devices can, therefore, offer an excellent tuning range and an inherent combination of all beams in a single waveguide.

5. Monolithic beam combiners applied to DFB arrays

In order to simplify the beam combination of DFB arrays, monolithic beam combination of DFB array has been considered in [55, 56]. These beam combiners are interesting for integration of the QCL sources to stand-off systems, but unfortunately they exhibit low power efficiencies. In the following we will present the two most relevant approaches one can consider for monolithic beam combiner design: (a) achromatic beam combiners, where the trade-off between the single transverse mode emission and the power efficiency (keeping the single transverse emission) should be considered. This has however the advantage of design simplicity. (b) Spectrally selective beam combination with more complicated designs that limits the practically achievable power efficiencies.

An array of sampled grating DFBs with monolithic beam-combiner was reported at wavelengths between 6 to 10 μm in [56]. The 21 targeted lasing channels were realized through 8 sampled grating DFB QCLs, exploiting the advantage of the sampled grating DFB design in order to reduce the number of the elements of a DFB array. These arrays with 8 DFB QCLs were beam combined to a single output using a three-stage Y-junction and S-bend waveguides. The last Y-junction was replaced with a two-in-one funnel combiner in order to suppress the higher order modes (see figure 7(a)). The grating periodicity was varied over 8 laser ridges from 0.97 to 1.40 μm in order to cover the bandwidth of 520 cm^{-1}, where each laser ridge provides Vernier tuning between 45 to 65 cm^{-1}. While the peak power of DFB array realized on the same active region exceeds ∼300 mW (see figure 3), the maximum peak power of the monolithically beam combined array was below 5 mW. This difference in the performance was attributed to the significantly higher threshold of the sampled grating DFB QCLs as compared to DFB QCLs (∼2.2 times higher) and the transmission losses in the beam combiner region. Despite the careful design of the beam combiner waveguide in order to suppress the transverse modes, the combined arrays did not show great spectral properties evident by the strong variation of the SMSR from few dB to >20 dB over the operating bandwidth (see figure 7(b)). This laser source was employed in a proof of principle spectroscopy application for measurement of the broadband absorption spectrum of methane [56].

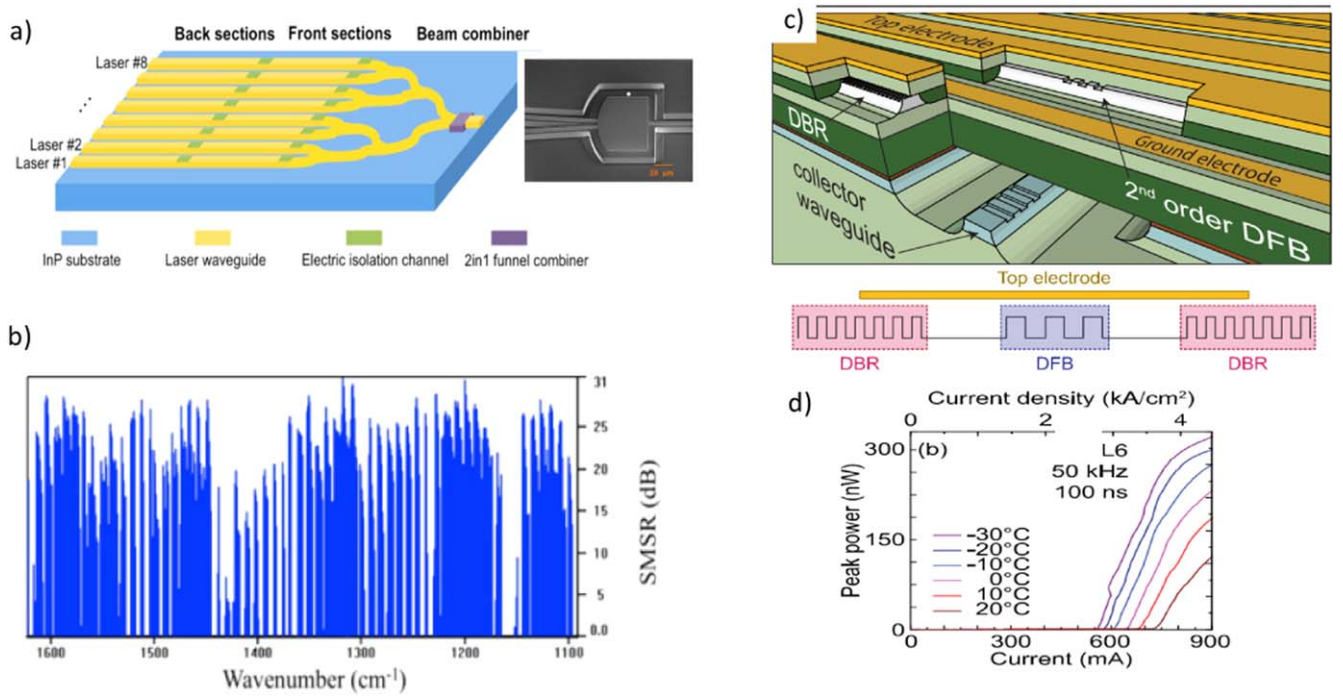

Figure 7. (a) Schematic drawing of chip consisting of the buried heterostructure lasers, bonded to the collector waveguide. Text labels and sections reveal the functional elements. (b) LIV curves for one of the array elements at different temperature. (c) Schematic of the the integrated beam combined SGDFB laser array, as well as the SEM images of the two-in-one funnel combiner with Si_3N_4 passivation and openings on top of the waveguide. (d) SMSR as a function of wavenumber, from automatic continuous tuning measurements. ((a)–(b) adapted from [55], (c)–(d) adapted from [56]. CC BY 4.0.

Our group demonstrated the use of second-order DFB gratings in order to extract and recombine the emission of an array of DFB QCLs to a single waveguide (see figure 7(c)) [55]. The proof of principle of functionality was demonstrated with spectral coverage of 170 cm^{-1} but with an estimated peak power $<$ few μW [55] due to losses and coupling efficiency of couplers (see figure 7(d)). Thermal performance of the device, comprising of two wafer-bonded chips, was another limiting factor in its final performance.

In summary, the so far reported monolithic integration of beam combiners to DFB QCL arrays are limited by either their high side mode suppression ratio (strong variation of SMSR from few dB to $>$20 dB [56]) or by their low output peak powers ($<$ few μW in pulse [55]).

6. Dual-wavelength DFB QCLs

An alternative approach to an array of emitter equally spaced in frequencies is to select specific windows of interest in the mid-IR spectrum and probe the gases with a few multi-wavelength QCLs, more specifically dual-wavelength DFB QCLs [57, 58]. This approach simplifies the optical layout of the final multi-species gas spectrometer, and at the same time allows optimizing the device performance of dual-wavelength sources with more design freedom. The targeted spectral regions cover the whole mid-IR spectrum from 4.25 μm to 9.5 μm with six narrow spectral windows, each one having a bandwidth of few cm^{-1} that is defined by the tuning range of DFB QCLs. Within these six narrow window, 10 of the most important pollutant and greenhouse gases (NH_3, O_3, NO, NO_2, CO, N_2O, H_2O, CH_4 and CO_2[^{12}C and ^{13}C]) have strong absorption lines that can be measured. The latest demonstration of the spectrometer used two dual-wavelength DFB QCLs and one single wavelength DFB QCLs, but the design can be easily adapted to three dual-wavelength DFB-QCLs. Using three dual-wavelength DFB QCLs instead of six single wavelength DFB QCLs has the advantage of a great reduction of the complexity for combination optics needed to guide the beams through the same interaction volume and onto the detector [18]. For details see the next section on the spectroscopy results using dual-wavelength DFB QCLs.

Our group demonstrated the first sequentially operating pulsed dual-wavelength QCL with electrically separated laser sections, emitting single-mode at 5.25 and 6.25 μm in 2014 [59]. Based on a single waveguide ridge, this laser represented a considerable asset to optical sensing and trace gas spectroscopy, as it allows probing multiple gas species with spectrally distant absorption features using conventional optical setups without any beam combining optics. Initial gas spectroscopy results demonstrated for simultaneous NO and NO_2 detection, reaching sub-ppb detection limits and selectivity comparable to conventional high-end spectroscopic systems.

Motivated by these encouraging results we developed three designs for dual-wavelength lasers allowing electrically switching between different wavelengths: (i) Dual section DFB QCLs, (ii) Neighbor DFB QCLs, (iii) Dual-wavelength

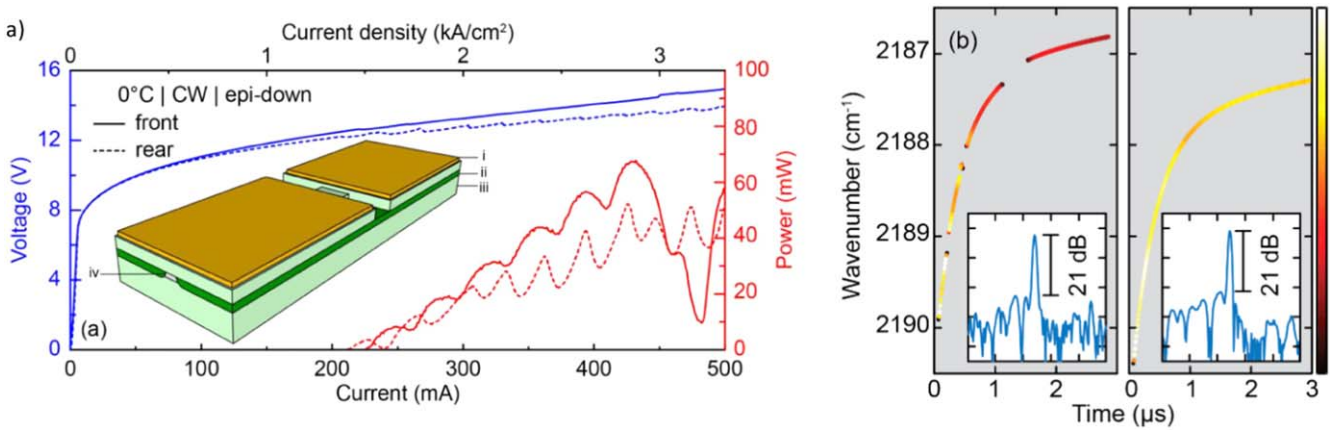

Figure 8. (a) LIV characteristic of a dual section DFB QCL at 4.34 μm and 4.56 μm with a device schematic in the inset. The threshold and slope efficiency of both lasing modes are quite well balanced. (b) Time-resolved mode maps of a dual-section DFB operated operated in intermittent continuous wave before (left panel) and after (right panel) anti-reflective coating. The spectra in the inset show that the SMSR in intermittent continuous wave before and after anti-reflective coating is >21 dB. Adapted from [57]. CC BY 4.0.

Vernier switching and tuning DFB QCls. The first two designs have been successfully employed in intermittent continuous wave mode operation [60] with a repetition rate of about 1kHz for each device, where the results of atmospheric measurements of the greenhouse gases (CO_2, N_2O, CH_4, and H_2O), and the pollutant gases (CO, NO, NO_2,O_3, SO_2 and NH_3) in a single optical setup will be summarized.

The first dual-wavelength targets 2190 and 2281 cm^{-1} to detect CO_2 (including its major isotopologues), CO and N_2O gases [57]. The design consists of two DFB lasers with QWS structure for better control over the mode selection, implemented on a single ridge device. The electrical isolation of the two sections were realized by a shallow etch trench between the two section. Dual-section DFBs at 4.34 and 4.56 μm had quite similar performance, as shown by the comparable threshold currents and slope efficiencies for both sections in continuous wave driving condition in figure 8(a). The power modulation as a function of injected current observed in these devices was attributed to the internal etaloning effect, where the temperature profile varies along the laser ridge, and hence the effective refractive index (n_{eff}) causes change in the cavity resonances for the back and front section. This etaloning effect has a strong impact on both frequency tuning and output power of the laser. This effect was considerably reduced by applying anti-reflective coating on the front facet of the laser [57]. The time-resolved measurements also showed the mode-hop free tuning and smooth variation of the laser intensity when driving the laser in intermittent continuous wave mode (see figure 8(b)). The initial spectroscopy results using dual-section QCLs at 5.26 and 6.25 μm are shown in [59] for NO and NO_2 detection, reaching sub-ppb detection limits. Later on in [57], the simultaneous measurements of the gases CO_2, CO and NO_2 were reported with a precision of 0.055 ppb, 0.042 ppb, and 0.075 ppm (at 60 s integration time), respectively, using devices at 4.25 and 4.55 μm.

Another design of dual-wavelength DFB QCLs demonstrated by our group is called neighbor DFB (NDFB) QCLs, consists of two electrically isolated DFB QCLs integrated side by side, where each one lasing at different wavelength. This design can be considered as a simpler version of DFB QCL arrays, where each of the QCLs targets a well defined lasing frequency that can be in our case 300 cm^{-1} apart from each other. The spacing between DFB QCLs can be as small as 20–35 μm, the limit being given by the minimum practical spacing required between the ridges for the standard buried heterostructure fabrication process [11]. This design has been successfully shown for two mid-IR windows, i.e. 5.26 and 6.25 μm as well as 7.4 and 9.5 μm [58] (see figure 9 for the results at 7.4 and 9.5 μm). The advantage of this design over DFB arrays is the small spacing that allows for a standard packaging optics, e.g. High Heat Load (HHL) packaging, with a collimating lens of focal distance of $f = 4$ mm to have a very small pointing angle error as 5 mrad. The latter value is comparable to the best value achieved for beam combination of DFB arrays using a single grating [43].

The spacing of the NDFB beams has been measured at the center of a 76-m-long multipass cell to be about 2.3 mm. The width of the dual beam at the entrance to the multipass cell was about the same size as the coupling hole of the cell, which has a diameter of 4.2 mm. Therefore, the beam of the NDFB was able to be focused on a single detector at output. This is indeed of crucial importance as it allows integration of these devices without complicated beam combining optics. This design was used at 1600 and 1900 cm^{-1} in [18] for measuring NO and NO_2 gases with 0.4 ppb and 0.1 ppb precision, respectively, for an integration time corresponding to the minimum of an Allan-Werle deviation plot.

Moreover, the NDFB design offers extension of the tuning range up to ~10 cm^{-1} using the neighbor laser as an integrated heater similar to the demonstrated extended tuning DFB QCLs with integrated heater [61]. The temperature-tuning coefficient of $\beta = \frac{1}{\lambda}\frac{d\lambda}{dT} \sim 7 \times 10^{-5}\,K^{-1}$ for the NDFBs [58] make them suitable for other techniques for trace gas sensing like wavelength/frequency modulation spectroscopy [62, 63] or photoacoustic spectroscopy [64].

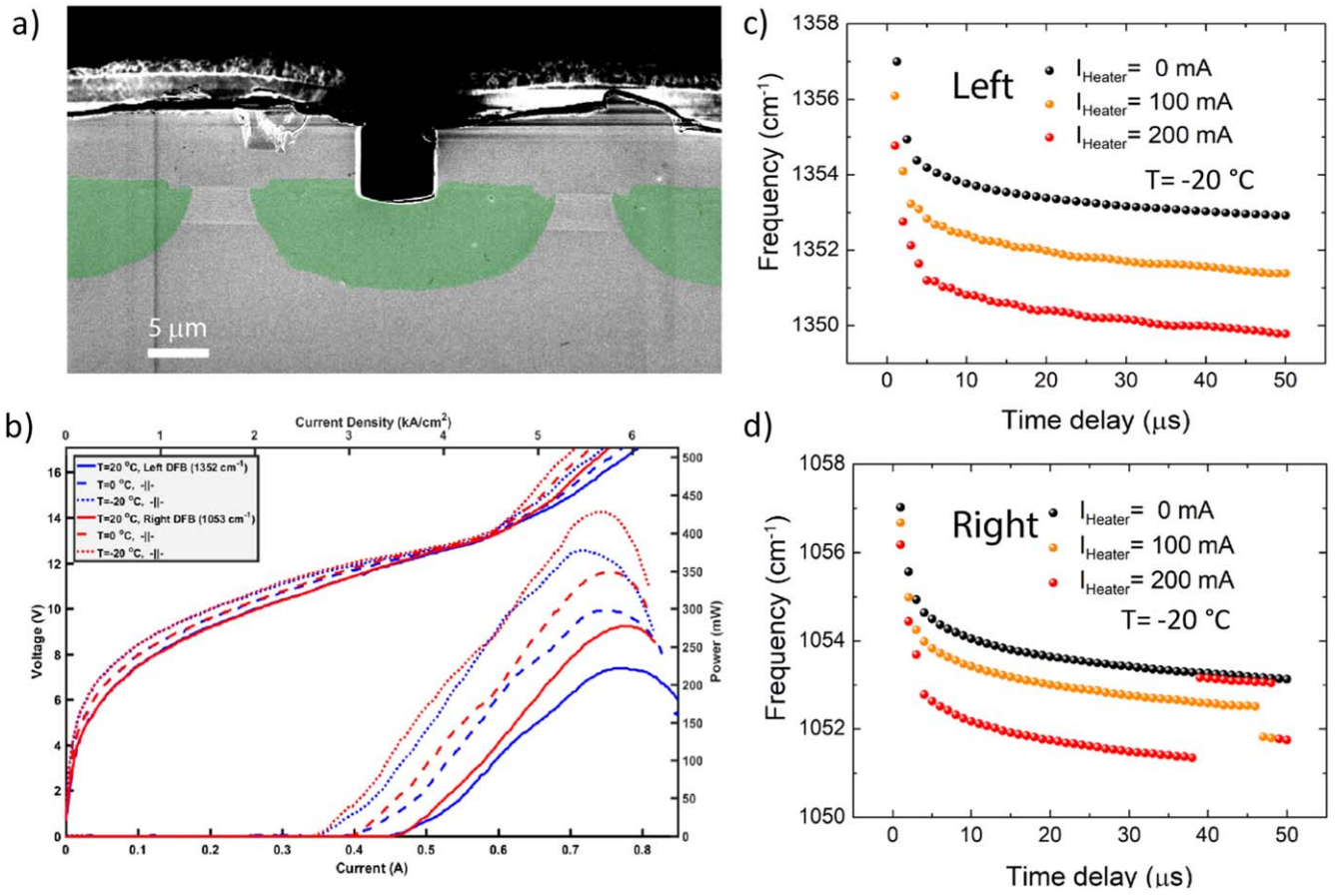

Figure 9. (a) SEM image of the front facet of a NDFB QCL pair, with center-to-center distance of the laser ridges of 30 μm. Green color indicates the insulating InP: Fe cladding layer. (b) LIV characteristics of a 2.5 mm long HR-coated laser of the same NDFB pair, at 1% duty cycle for 100-ns long pulses for substrate temperatures of −20, 0, and 20 °C. (c-d) Tuning of the emission mode frequency for the left and right DFB, respectively, over long pulses of 50 μs applied with duty cycle of 25%, as a function of time delay over the pulse and for three different values of the continuous wave bias current applied on the neighboring laser. Adapted from [58]. CC BY 4.0.

Both dual-section and NDFB QCLs have been successfully realized and employed in a compact multi-species gas spectrometer with a small footprint of 45 × 45 cm^2. To try and alleviate the limitations of the previous designs, that is the pointing error of the NDFB QCLs and the etaloning of the dual-section devices, we have investigated Vernier switching and tuning DFB QCLs [58] as another option to realize dual-wavelength DFB QCLs. The Vernier effect was exploited on digitized gratings [65], that allows switching between DFB modes that are 300 cm^{-1} apart. Frequency tuning was thermally induced by two heater sections, which are made from wide ridges of the active region etched in close proximity to the laser ridges (see inset of figure 10(a)). The heaters in this design are electrically isolated from the laser ridge which can be beneficial for other spectroscopy techniques such as frequency modulated spectroscopy. The front and back heater sections are separated by a narrow dry-etched trench that allows efficient tuning as well as electrical isolation between them. The active region gain was designed such that it is balanced around the wavelengths of laser emission. The wavelength switching was successfully demonstrated for short pulses as shown in figures 10(b) and (c). The LIV characteristics of the device shows higher threshold for the switched channel, i.e. the lasing channel that requires thermal tuning of the mirror reflectivity. When the front heater is not driven, and the device is aligned to the 1600 cm^{-1} channel, good intermittent continuous wave performance is demonstrated, evident by the mode-hop free tuning over the whole 15 μs pulse. For the 1900 cm^{-1} channel, however, intermittent continuous wave performance was limited to pulses shorter than 1 μs. This limited operation mainly comes from the thermal management of the device, which has to handle the heat load coming from the large ridge width of the laser section as well as the increased temperature of the laser ridge by approximately 27 °C caused by the power dissipation of the heater. One should also consider the self-heating effect that is expected to be $\geqslant$30 °C in the first 500 ns of the applied pulse. Improvement of the efficiency of the active region, better thermal management of the laser by fabricating narrower ridges, or reducing the optical losses of the cavity by waveguide design may further improve the Vernier based DFB QCLs. Integration of the gain section in the middle of the device would reduce the thermal heating of the gain when activating the heaters for switching. This may help increasing the maximum operating temperature and should be considered for further realization of such devices.

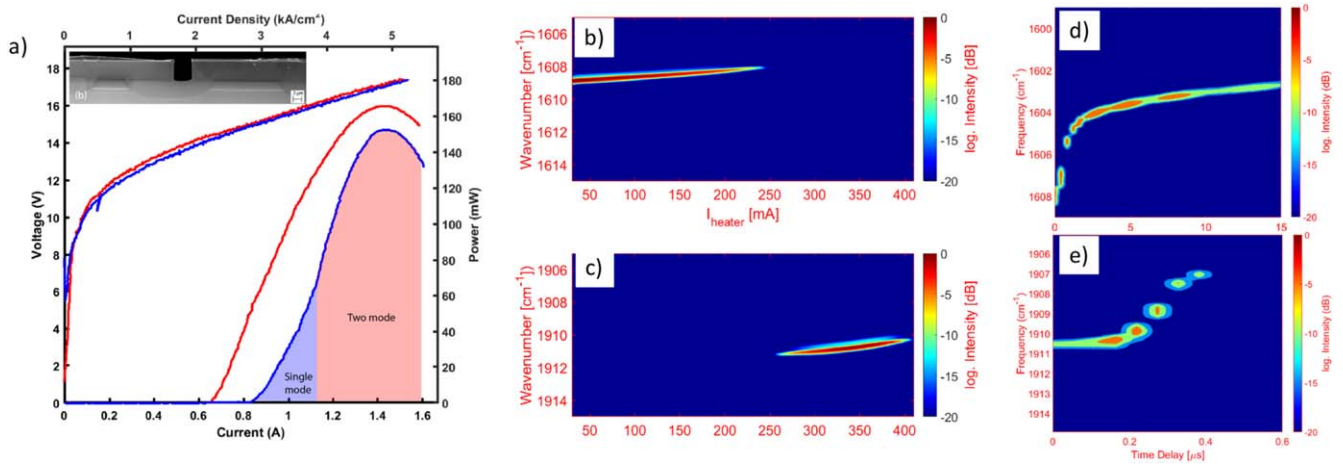

Figure 10. (a) LIV characteristics of an anti-reflective-coated Vernier DFB QCL with ridge width of 8 μm and length 3.5 mm, for two different values of the heater bias current ($I_{Heater} = 0$ mA (red) and $I_{Heater} = 348$ mA (blue)), corresponding to lasing at either of the target channels. Substrate temperature is T $= -20$ °C and the device is driven with 100 ns pulses at 1% duty cycle. The heater is biased with continuous wave current of 348 mA, corresponding to the power dissipation of 3.7 W. The blue and pink areas under the L-I curve during front heater operation, correspond to the single mode or double mode operation regime. Inset: SEM image of the cross-section of a Vernier based switching dual-wavelength DFB QCL. (b), (c) Spectral map of the two channels as a function of the heat continuous wave bias-current. The laser is driven by 30-ns long pulses, at a period of 10 μs, and a bias current of 1000 mA. Switching starts at a heater bias current of 250 mA, corresponding to 2.67 W of dissipated power and full alignment occurs when heater current bias is 346 mA, or 3.7 W of power are dissipated. (d), (e) The intermittent continuous wave operation of the Vernier QCL device, ($P_{heater} = 0$ and 3.7 W for the upper and lower panel). Whereas, both maps show the mod-hop free tuning of the laser with high SMSR, the 1900 cm^{-1} channel is limited in lasing up to few 100s of ns. Adapted from [58]. CC BY 4.0.

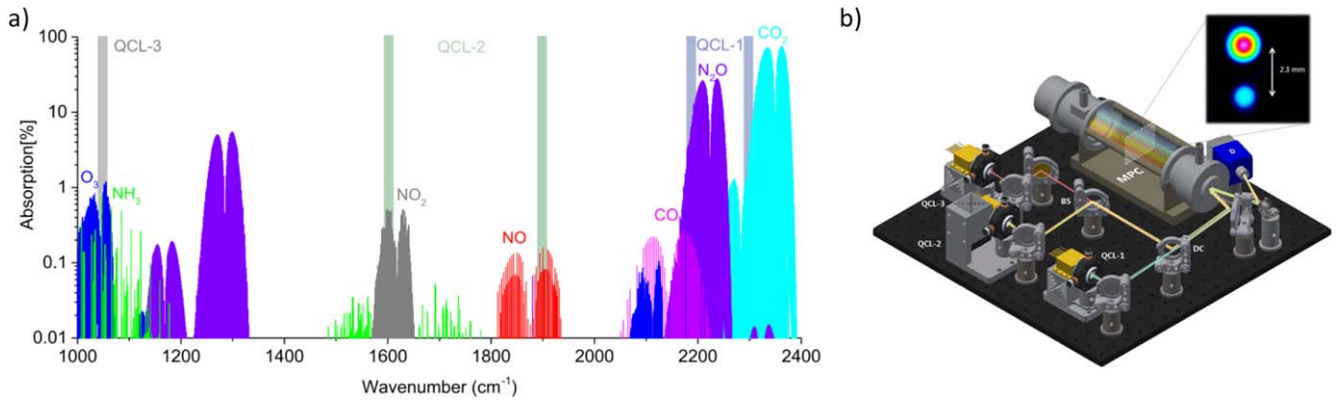

Figure 11. (a) Simulated absorption of the target gases for typical ambient mole fractions (O_3: 100 ppb; NH_3: 5 ppb; NO_2: 100 ppb; NO: 50 ppb; CO: 150 ppb; N_2O: 330 ppb; CO_2: 400 ppm), considering 76 m optical path length, 80 hPa, and 296 K. The shaded areas mark the frequencies used in [18]. The shading colors indicate the three different device types. (b) schematic model of the optical layout of the multi-laser instrument. The beams of three QCLs are combined using a dichroic (DC) and a CaF_2 beam splitter (BS) before the merged beam is coupled into a 76-m-long multipass absorption cell (MPC) and focused on the detector (D). The type of QCL sources used are: QCL-1 (Single DFB QCL), QCL-2(NDFB QCL), and QCL-3 (Dual-section DFB QCL). The inset (top-right) shows an IR beam profile of the NDFB QCL (QCL-2) recorded at 55cm distance, corresponding to the center of the multipass cell. Adapted from [18].

7. Multi-species trace gas sensing with dual-wavelength QCLs

The dual-section and NDFB QCLs presented as dual-wavelength DFB QCLs have been successfully employed in a mid-infrared laser absorption spectrometer [18]. Figure 11(a) summarizes the choice of five target frequencies along with the corresponding species. These selections represent a good compromise between maximal line strength, minimal interference from water vapor, and the objective to cover several target molecules within the scanning range of every laser. A schematic of the optical layout for the multi-laser instrument is shown in figure 11(b). The divergent outputs of the QCLs are focused with aspheric lenses with focal length $f = 6$mm such that their beam-waist is matched to the multipass cell (AMAC-76, Aerodyne Research Inc.). The beams are combined using a custom dichroic (optimized for reflection at $\lambda = 4$ μm and transmittance at $\lambda > 5$ μm) and a wedged CaF_2 beam splitter (BSW510, Thorlabs). The beam exiting the multipass cell is then focused onto a thermoelectrically cooled MCT detector (PVM-4TE-8, Vigo Systems, S.A.) using a spherical mirror with a focal length of 75 mm.

The lasers are driven time-multiplexed in intermittent continuous wave mode with a repetition rate of 1 kHz [66].

Table 1. Summary of Allan-Werle deviations representing the 1σ limit of detection and the corresponding absorption noise given after 1s integration time and at the Allan deviation minimum ('best'), which was typically reached between 100 and 300 s integration time. Adapted from [18], with permission of Springer.

Species	Precision (ppb)		Absorption noise		DFB-QCL type
	1s	Best	1s	Best	
CO	0.35	0.08	9.2E-0.5	2.1E-05	Dual-section
N_2O	0.49	0.045	9.9E-05	9.0E-06	Dual-section
CO_2	170	100	1.6E-04	9.3E-04	Dual-section
$\delta^{13}CO_2$	0.9	0.28	—	—	Dual-section
NO	3	0.4	1.7E-04	2.2E-05	NDFB
NO_2	0.8	0.1	1.6E-04	2.0E-05	NDFB
O_3	1.7	0.11	3.2E-05	2.0E-06	Single-DFB
NH_3	0.1	0.016	3.0E-05	4.8E-06	Single-DFB

The individual spectra are real-time averaged (1 s) by an FPGA-based data acquisition system. The combination of two dual- and one single-DFB QCL yields high-precision measurements of CO (0.08 ppb), CO_2 (100 ppb), NH_3 (0.02 ppb), NO (0.4 ppb), NO_2 (0.1 ppb), N_2O (0.045 ppb), and O_3 (0.11 ppb) simultaneously in a compact setup (45×45 cm^2). The summary of Allan-Werle deviations representing the 1σ limit of detection and the corresponding absorption noise given after 1 s integration time and at the Allan deviation minimum ('best'), which was typically reached between 100 and 300 s integration time, are summarized in table 1. The instrument was assessed for environmental monitoring and benchmarked with reference instrumentation to demonstrate its potential for compact multi-species trace gas sensing.

8. Conclusion

We reviewed the progress in realization of multi-wavelength DFB QCLs for broadband gas spectroscopy in the mid-IR spectrum. Most of the DFB QCL arrays reported so far suffer from the strong variation of the performance, i.e. the output power and deterministic lasing frequency, over their operation optical bandwidth. These issues have been addressed in MOPA DFB arrays, where high peak powers and almost uniform performance were demonstrated. While these designs cover a wide bandwidth of $\sim$100–200 cm^{-1}, high-resolution spectroscopy remains challenging because it typically requires deterministic control over the lasing frequency and mode-hop free tuning. Although, these sources achieve a spectral coverage nd quasi-continuous wavelength tuning, that is comparable to external cavity QCLS, the difficulties in beam combination limits their application. Vernier-switching DFB QCLs are an attractive alternative to DFB arrays, because several wavelengths can be multiplexed on a single ridge. However, Vernier-switching DFB QCL sources without integrated heaters require complicated driving electronics for continuous tuning. The Vernier-switching DFB QCLs with integrated heaters were realized on a single stack active regions with high performance. These sources can be considered as an alternative to conventional DFB arrays, since a relatively high number of modes can be multiplexed on a single ridge.

Using multiple dual-wavelength sources was considered as another approach by our group for high-precision trace-gas spectroscopy over broad optical bandwidth (from 4.25 to 9.5 μm). These sources allow considerable simplification of the final multi-species gas spectrometer, and most importantly allow exploiting the narrow linewidth feature of DFB QCLs. The three designs reviewed in this article (dual-section, NDFB, and Vernier DFB QCLs) provide great freedom in optimization of both active region performance and anti-reflective coatings. Moreover they allow equalizing the performance of the lasers over the target optical bandwidth. The dual-wavelength Vernier DFB QCLs were shown to have full wavelength switching in short pulses. However, the intermittent continuous wave operation was limited on the switched channel because its average temperature of the active region is higher. Improvement of the output power efficiency of Vernier based switching devices is required before employing them to high-resolution gas-trace spectroscopy. In the current design, the performance of the active region is reduced by the heaters which are required for mode selection. Placing the gain sections in the middle of the device and designing short mirror sections on both ends of the Vernier tuning devices may significantly improve the performance of these devices. The combination of the first two dual-wavelength design and one single-DFB QCL in a small footprint multi-species trace gas spectrometer [18] yields high precision measurements of CO (0.08 ppb), CO_2 (100 ppb), N_2O (0.045 ppb) (measured with dual-section DFB QCLs), and NO (0.4 ppb) and NO_2 (0.1 ppb) (measured with NDFB QCLs). This approach reduces the footprint and cost by replacing several instruments, while delivering direct, selective, and precise measurements of many target molecules.

Acknowledgments

We thank Dr Bo Meng, Dr Ruijun Wang and Dr Martin Franckie for careful reading and discussions. This work was supported by the SNF Bridge foundation under project 'Combtrace'.

ORCID iDs

Mehran Shahmohammadi https://orcid.org/0000-0002-6168-3365

References

[1] Faist J, Capasso F, Sivco D, Sirtori C, Hutchinson A and Cho A 1994 Quantum cascade laser *Science* **264** 553–6

[2] Kohler R, Tredicucci A, Beltram F, Beere H, Linfield E, Davies A, Ritchie D, Iotti R and Rossi F 2002 Terahertz semiconductor-heterostructure laser *Nature* **417** 156–9

[3] Gmachl C, Sivco D, Colombelli R, Capasso F and Cho A 2002 Ultra-broadband semiconductor laser *Nature* **415** 883–7

[4] Hugi A, Maulini R and Faist J 2010 External cavity quantum cascade laser *Semicond. Sci. Technol.* **25** 083001

[5] Lee B G, Zhang H A, Pfluegl C, Diehl L, Belkin M A, Fischer M, Wittmann A, Faist J and Capasso F 2009 Broadband distributed-feedback quantum cascade laser array operating from 8.0 to 9.8 μm *IEEE Photon. Technol. Lett.* **21** 914–6

[6] Rauter P, Menzel S, Goyal A K, Wang C A, Sanchez A, Turner G and Capasso F 2013 High-power arrays of quantum cascade laser master-oscillator power-amplifiers *Opt. Express* **21** 4518–30

[7] Song S, Howard S S, Liu Z, Dirisu A O, Gmachl C F and Arnold C B 2006 Mode tuning of quantum cascade lasers through optical processing of chalcogenide glass claddings *Appl. Phys. Lett.* **89** 041115

[8] Aellen T, Maulini R, Terazzi R, Hoyler N, Giovannini M, Faist J, Blaser S and Hvozdara L 2006 Direct measurement of the linewidth enhancement factor by optical heterodyning of an amplitude-modulated quantum cascade laser *Appl. Phys. Lett.* **89** 091121

[9] Bartalini S, Borri S, Galli I, Giusfredi G, Mazzotti D, Edamura T, Akikusa N, Yamanishi M and Natale P D 2011 Measuring frequency noise and intrinsic linewidth of a room-temperature dfb quantum cascade laser *Opt. Express* **19** 17996–8003

[10] Tombez L, Di Francesco J, Schilt S, Di Domenico G, Faist J, Thomann P and Hofstetter D 2011 Frequency noise of free-running 4.6 μm distributed feedback quantum cascade lasers near room temperature *Opt. Lett.* **36** 3109–11

[11] Beck M, Hofstetter D, Aellen T, Faist J, Oesterle U, Ilegems M, Gini E and Melchior H 2002 Continuous wave operation of a mid-infrared semiconductor laser at room temperature *Science* **295** 301–5

[12] Weidmann D, Tittel F, Aellen T, Beck M, Hofstetter D, Faist J and Blaser S 2004 Mid-infrared trace-gas sensing with a quasi-continuous-wave Peltier-cooled distributed feedback quantum cascade laser *Applied Physics B-Lasers And Optics* **79** 907–13

[13] Cristescu S, Persijn S, te Lintel Hekkert S and Harren F 2008 Laser-based systems for trace gas detection in life sciences *Appl. Phys.* B **92** 343

[14] Tuzson B, Zeyer K, Steinbacher M, McManus J B, Nelson D D, Zahniser M S and Emmenegger L 2013 Selective measurements of NO, NO_2 and NO_y in the free troposphere using quantum cascade laser spectroscopy *Atmos. Meas. Tech.* **6** 927–36

[15] Nelson D D, McManus B, Urbanski S, Herndon S and Zahniser M S 2004 High precision measurements of atmospheric nitrous oxide and methane using thermoelectrically cooled mid-infrared quantum cascade lasers and detectors *Spectrochim. Acta, Part A* **60** 3325–35

[16] Li J, Deng H, Sun J, Yu B and Fischer H 2016 Simultaneous atmospheric CO, n2o and h2o detection using a single quantum cascade laser sensor based on dual-spectroscopy techniques *Sensors Actuators* B **231** 723–32

[17] Lee B H, Wood E C, Zahniser M S, McManus J B, Nelson D D, Herndon S C, Santoni G W, Wofsy S C and Munger J W 2011 Simultaneous measurements of atmospheric hono and no2 via absorption spectroscopy using tunable mid-infrared continuous-wave quantum cascade lasers *Appl. Phys.* B **102** 417–23

[18] Hundt P M, Tuzson B, Aseev O, Liu C, Scheidegger P, Looser H, Kapsalidis F, Shahmohammadi M, Faist J and Emmenegger L 2018 Multi-species trace gas sensing with dual-wavelength qcls *Appl. Phys.* B **124** 108

[19] Bandyopadhyay N, Chen M, Sengupta S, Slivken S and Razeghi M 2015 Ultra-broadband quantum cascade laser, tunable over 760 cm^{-1}, with balanced gain *Opt. Express* **23** 21159–64

[20] Riedi S, Hugi A, Bismuto A, Beck M and Faist J 2013 Broadband external cavity tuning in the 3–4 μm window *Appl. Phys. Lett.* **103** 031108

[21] Ostendorf R *et al* 2016 Recent advances and applications of external cavity-qcls towards hyperspectral imaging for standoff detection and real-time spectroscopic sensing of chemicals *Photonics* **3** 28

[22] Mujagic E, Schwarzer C, Yao Y, Chen J, Gmachl C and Strasser G 2011 Two-dimensional broadband distributed-feedback quantum cascade laser arrays *Appl. Phys. Lett.* **98** 141101

[23] Jouy P, Bonzon C, Wolf J, Gini E, Beck M and Faist J 2015 Surface emitting multi-wavelength array of single frequency quantum cascade lasers *Appl. Phys. Lett.* **106** 071104

[24] Liu P Q, Wang X and Gmachl C F 2012 Single-mode quantum cascade lasers employing asymmetric mach-zehnder interferometer type cavities *Appl. Phys. Lett.* **101** 161115

[25] Hugi A, Villares G, Blaser S, Liu H C and Faist J 2012 Mid-infrared frequency comb based on a quantum cascade laser *Nature* **492** 229–33

[26] Villares G, Hugi A, Blaser S and Faist J 2014 Dual-comb spectroscopy based on quantum-cascade-laser frequency combs *Nat. Commun.* **5** 1–9

[27] Jouy P, Wolf J M, Bidaux Y, Allmendinger P, Mangold M, Beck M and Faist J 2017 Dual comb operation of 8.2 μm quantum cascade laser frequency comb with 1 w optical power *Appl. Phys. Lett.* **111** 141102

[28] Coddington I, Newbury N and Swann W 2016 Dual-comb spectroscopy *Optica* **3** 414–26

[29] Westberg J, Sterczewski L A, Kapsalidis F, Bidaux Y, Wolf J M, Beck M, Faist J and Wysocki G 2018 Dual-comb spectroscopy using plasmon-enhanced-waveguide dispersion-compensated quantum cascade lasers *Opt. Lett.* **43** 4522–5

[30] Lyakh A, Barron-Jimenez R, Dunayevskiy I, Go R and Patel C K N 2015 External cavity quantum cascade lasers with ultra rapid acousto-optic tuning *Appl. Phys. Lett.* **106** 141101

[31] Wittmann A, Giovannini M, Faist J, Hvozdara L, Blaser S, Hofstetter D and Gini E 2006 Room temperature, continuous wave operation of distributed feedback quantum cascade lasers with widely spaced operation frequencies *Appl. Phys. Lett.* **89** 141116

[32] Lee B G *et al* 2007 Widely tunable single-mode quantum cascade laser source for mid-infrared spectroscopy *Appl. Phys. Lett.* **91** 231101

[33] Lee B G *et al* 2009 Dfb quantum cascade laser arrays *IEEE J. Quantum Electron.* **45** 554–65

[34] Rauter P and Capasso F 2015 Multi-wavelength quantum cascade laser arrays *Laser Photonics Rev.* **9** 452–77

[35] Lee B G, Zhang H A, Pflugl C, Diehl L, Belkin M A, Fischer M, Wittmann A, Faist J and Capasso F 2009 Broadband distributed-feedback quantum cascade laser array operating from 8.0 to 9.8 μm *IEEE Photonics Technol. Lett.* **21** 914–6

[36] Rauter P, Menzel S, Goyal A K, Wang C A, Sanchez A, Turner G and Capasso F 2013 High-power arrays of quantum cascade laser master-oscillator power-amplifiers *Opt. Express* **21** 4518–30

[37] Rauter P, Menzel S, Goyal A K, Gökden B, Wang C A, Sanchez A, Turner G W and Capasso F 2012 Master-oscillator power-amplifier quantum cascade laser array *Appl. Phys. Lett.* **101** 261117

[38] Usami M, Akiba S and Utaka K 1987 Asymmetric /4-shifted ingaasp/inp dfb lasers *IEEE J. Quantum Electron.* **23** 815–21

[39] Utaka K, Akiba S, Sakai K and Matsushima Y 1986 /4-shifted ingaasp/inp dfb lasers *IEEE J. Quantum Electron.* **22** 1042–51

[40] Rauter P, Menzel S, Gokden B, Goyal A K, Wang C A, Sanchez A, Turner G and Capasso F 2013 Single-mode tapered quantum cascade lasers *Appl. Phys. Lett.* **102** 181102

[41] Williams R *et al* 1999 Kilohertz linewidth from frequency-stabilized mid-infrared quantum cascade lasers *Opt. Lett.* **24** 1844–6

[42] Rauter P, Menzel S, Gokden B, Goyal A K, Wang C A, Sanchez A, Turner G and Capasso F 2013 Single-mode tapered quantum cascade lasers *Appl. Phys. Lett.* **102** 181102

[43] Lee B G, Kansky J, Goyal A K, Pflügl C, Diehl L, Belkin M A, Sanchez A and Capasso F 2009 Wavelength beam combining of quantum cascade laser arrays for remote sensing *Lidar Remote Sensing for Environmental Monitoring* X **7460** 746004 International Society for Optics and Photonics

[44] Goyal A K, Spencer M, Shatrovoy O, Lee B G, Diehl L, Pfluegl C, Sanchez A and Capasso F 2011 Dispersion-compensated wavelength beam combining of quantum-cascade-laser arrays *Opt. Express* **19** 26725–32

[45] Szedlak R *et al* 2017 Surface emitting ring quantum cascade lasers for chemical sensing *Opt. Eng.* **57** 57

[46] Szedlak R *et al* 2016 Remote sensing with commutable monolithic laser and detector *ACS Photonics* **3** 1794–8

[47] Jayaraman V, Chuang Z M and Coldren L A 1993 Theory, design, and performance of extended tuning range semiconductor lasers with sampled gratings *IEEE J. Quantum Electron.* **29** 1824–34

[48] Todt R, Jacke T, Laroy R, Morthier G and Amann M C 2005 Demonstration of vernier effect tuning in tunable twin-guide laser diodes *IEE Proceedings—Optoelectronics* **152** 66–71

[49] Kalchmair S, Blanchard R, Mansuripur T S, de Naurois G-M, Pfluegl C, Witinski M F, Diehl L, Capasso F and Loncar M 2015 High tuning stability of sampled grating quantum cascade lasers *Opt. Express* **23** 15734–47

[50] Mansuripur T S, Menzel S, Blanchard R, Diehl L, Pflügl C, Huang Y, Ryou J-H, Dupuis R D, Loncar M and Capasso F 2012 Widely tunable mid-infrared quantum cascade lasers using sampled grating reflectors *Opt. Express* **20** 23339–48

[51] Slivken S, Bandyopadhyay N, Bai Y, Lu Q Y and Razeghi M 2013 Extended electrical tuning of quantum cascade lasers with digital concatenated gratings *Appl. Phys. Lett.* **103** 231110

[52] Lu Q Y, Slivken S, Bandyopadhyay N, Bai Y and Razeghi M 2014 Widely tunable room temperature semiconductor terahertz source *Appl. Phys. Lett.* **105** 201102

[53] Slivken S, Bandyopadhyay N, Tsao S, Nida S, Bai Y, Lu Q Y and Razeghi M 2012 Sampled grating, distributed feedback quantum cascade lasers with broad tunability and continuous operation at room temperature *Appl. Phys. Lett.* **100** 261112

[54] Bidaux Y, Bismuto A, Tardy C, Terazzi R, Gresch T, Blaser S, Muller A and Faist J 2015 Extended and quasi-continuous tuning of quantum cascade lasers using superstructure gratings and integrated heaters *Appl. Phys. Lett.* **107** 221108

[55] Süess M J, Jouy P, Bonzon C, Wolf J, Gini E, Beck M and Faist J 2016 Single-mode quantum cascade laser array emitting from a single facet *IEEE Photonics Technol. Lett.* **28** 1197–200

[56] Zhou W, Bandyopadhyay N, Wu D, McClintock R and Razeghi M 2016 Monolithically, widely tunable quantum cascade lasers based on a heterogeneous active region design *Sci. Rep.* **6** 25213

[57] Süess M J, Hundt P M, Tuzson B, Riedi S, Wolf J M, Peretti R, Beck M, Looser H, Emmenegger L and Faist J 2016 Dual-section dfb-qcls for multi-species trace gas analysis *Photonics* **3** 24

[58] Kapsalidis F, Shahmohammadi M, Süess M J, Wolf J M, Gini E, Beck M, Hundt M, Tuzson B, Emmenegger L and Faist J 2018 Dual-wavelength dfb quantum cascade lasers: sources for multi-species trace gas spectroscopy *Appl. Phys.* B **124** 107

[59] Jágerská J, Jouy P, Hugi A, Tuzson B, Looser H, Mangold M, Beck M, Emmenegger L and Faist J 2014 Dual-wavelength quantum cascade laser for trace gas spectroscopy *Appl. Phys. Lett.* **105** 161109

[60] Fischer M, Tuzson B, Hugi A, Brönnimann R, Kunz A, Blaser S, Rochat M, Landry O, Müller A and Emmenegger L 2014 Intermittent operation of qc-lasers for mid-ir spectroscopy with low heat dissipation: tuning characteristics and driving electronics *Opt. Express* **22** 7014–27

[61] Bismuto A, Bidaux Y, Tardy C, Terazzi R, Gresch T, Wolf J, Blaser S, Muller A and Faist J 2015 Extended tuning of mid-ir quantum cascade lasers using integrated resistive heaters *Opt. Express* **23** 29715–22

[62] Supplee J M, Whittaker E A and Lenth W 1994 Theoretical description of frequency modulation and wavelengthmodulation spectroscopy *Appl. Opt.* **33** 6294–302

[63] Bjorklund G C 1980 Frequency-modulation spectroscopy: a new method for measuring weak absorptions and dispersions *Opt. Lett.* **5** 15–7

[64] Sigrist M W 2003 Trace gas monitoring by laser photoacoustic spectroscopy and related techniques (plenary) *Rev. Sci. Instrum.* **74** 486–90

[65] Li Y, Xu M, Voirin G, Sixt P and Parriaux O M 1996 Experimental study of digitalized dual-frequency coupling gratings *Proc. SPIE 2891, Integrated Optoelectronics* **2891** 2891–3

[66] Liu C, Tuzson B, Scheidegger P, Looser H, Bereiter B, Graf M, Hundt M, Aseev O, Maas D and Emmenegger L 2018 Laser driving and data processing concept for mobile trace gas sensing: design and implementation *Rev. Sci. Instrum.* **89** 065107